J. Ocean Univ. China (Oceanic and Coastal Sea Research)
https://doi.org/10.1007/s11802-020-4352-1
ISSN 1672-5182, 2020 19 (6): 1315-1330
http://www.ouc.edu.cn/xbywb/
E-mail:xbywb@ouc.edu.cn

U-Pb Isotope Geochronology of Syntectonic Granites from Hainan Island, South China: Constraints on Tectonic Evolution of the Eastern Paleo-Tethys Ocean

ZHOU Yang[1), 2)], YAN Yi[1)], LIU Hailing[3), *], CAI Jianxin[3)], ZHOU Mengfei[4)], ZHANG Xinchang[1)], WANG Yin[2), 5)], and SHEN Baoyun[6)]

1) *Key Laboratory of Ocean and Marginal Sea Geology*, *Guangzhou Institute of Geochemistry*, *Chinese Academy of Sciences*, *Guangzhou* 510640, *China*
2) *University of Chinese Academy of Sciences*, *Beijing* 100049, *China*
3) *South China Sea Institute of Oceanology*, *Chinese Academy of Sciences*, *Guangzhou* 510301, *China*
4) *Institute of Porous Flow and Fluid Mechanics*, *Chinese Academy of Sciences*, *Langfang* 065007, *China*
5) *SKL*, *Institute of Geology and Geophysics*, *Chinese Academy of Sciences*, *Beijing* 100029, *China*
6) *School of Electromechanical Engineering*, *Guangdong University of Technology*, *Guangzhou* 510006, *China*

(Received October 10, 2019; revised May 3, 2020; accepted June 4, 2020)

Abstract Since the recognition of the Indosinian orogeny in northern Vietnam, Triassic orogens have been widely identified around the western and southwestern boundaries of the South China block. The paleo-Tethys sutures stretch from west to southeast, from Jinshajiang-Ailaoshan *via* NE Vietnam to Hainan Island; these sutures exhibit and develop voluminous Permian–early Triassic magmatism and numerous high-strain shear zones. As ophiolites related to the paleo-Tethys are lacking on Hainan Island, the eastward extension of the Indosinian orogeny and subduction and closure time of the paleo-Tethys Ocean on Hainan Island remain controversial. Here, an integrated kinematic and geochronological study has been conducted on two shear zones, called the Xiaomei and Mangsan shear zones. U-Pb zircon dating yields an age of early Triassic (252–251 Myr) for Xiaomei syntectonic granites which formed in the same tectonic setting and presented the similar nanoparticles to the Indosinian granites from Ailaoshan ductile shear zone, including the strawberry-like and flower-like nanoparticles. The NE-trending Mangsan shear zone represented by the gneissic granites with middle Permian ages (264–262 Myr) formed in the same tectonic setting as the Wuzhi-shan granites that were proposed as I-type granites. These middle Permian gneissic granites with arc affinity may represent an arc setting related to the NW subduction of the paleo-Tethys. The analyses reveal that granites with late Triassic ages (235–232 Myr) in the Xiaomei shear zone have the characteristics of A-type granites. The late Triassic extensional events on Hainan Island may be related to the subduction of the paleo-Pacific Plate beneath the East Asian continent.

Key words Indosinian orogeny; Hainan Island; Xiaomei shear zone; Mangsan shear zone; syntectonic granites; paleo-Tethys

1 Introduction

Hainan Island is located in the zone of convergence among the Philippine Plate, South China continent and Indochina block (Fig.1a). This island consists of several allochthonous continental blocks, which rifted from the northern margin of Gondwanaland, drifted northwards, and eventually amalgamated to form Hainan Island during the Paleozoic and Mesozoic (Metcalfe, 1996, 2017; Li *et al*., 2002; Liu *et al*., 2006). Due to its unique geotectonic location, it is undoubtedly the key to understanding the tectonic evolution of the Indochina block and the South China continent, especially the opening and closing of the eastern paleo-Tethyan branch in the late Paleozoic to early Mesozoic. In the South China continent, Triassic ductile shearing, plutonismand metamorphism related to the Indosinian orogeny are documented in the central and eastern China (Fig.1a; Lin *et al*., 2000; Faure *et al*., 2003, 2016; Mao *et al*., 2013). On the southern margin of the South China block, the Jinshajiang, Ailaoshan, and North Vietnam belts exhibit striking similarities, with the suture zoneshaving a Permian–early Triassic magmatic arc, an ophiolitic mélange, northeast to north-directed synmetamorphic ductile nappes, and a fold-and-thrust belt (Fig.1a; Faure *et al*., 2016). These belts represent Triassic orogens around the western and southwestern boundaries of the South China continent (Chen and Xie, 1994; Lepvrier *et al*., 2008; Fan *et al*., 2010; Liu *et al*., 2012). These collisional belts resulted from the closure of the paleo-Tethys and subsequent collision between the South China Plate and Indochina (Faure *et al*., 2016). Now questions arise as to

* Corresponding author. E-mail: liuh82@163.com

whether the Indosinian orogeny exists, and if so, when the paleo-Tethys closed on Hainan Island.

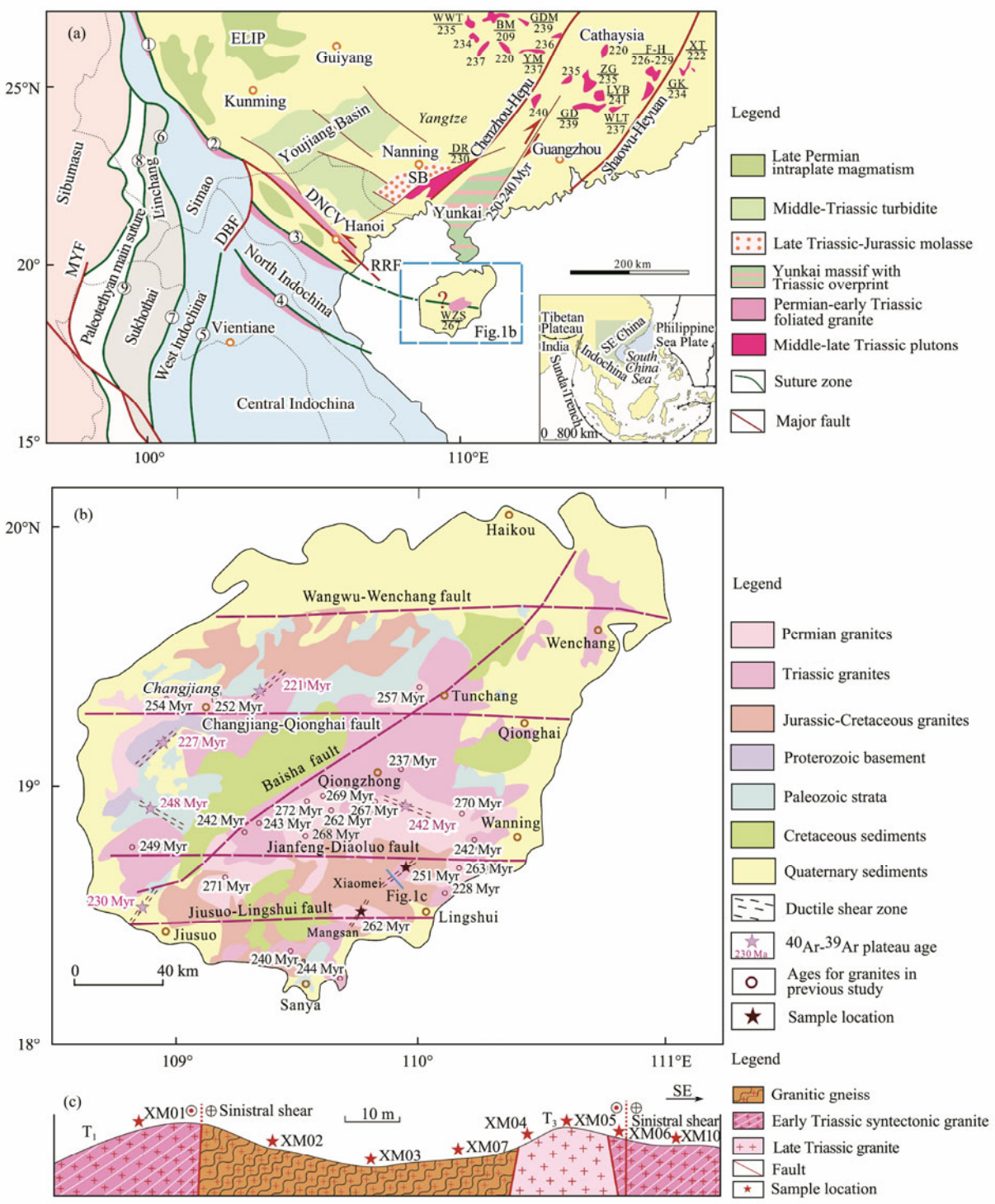

Fig.1 (a) Tectonic sketch map of Southeast Asia showing the major suture boundaries and tectonic fragments (modified after Li *et al*., 2002; Mao *et al*., 2013; Faure *et al*., 2016; Metcalfe, 2017; Wang *et al*., 2017). ELIP, Emeishan large igneous province; SB, Shiwandashan Basin; DNCV, Day Nui Con Voi Triassic arc; RRF, Red River fault; DBF, Dien Bien Phu fault; MYF, Mae Yuan fault. Major suture boundaries: 1, Jinshajiang suture; 2, Ailaoshan suture; 3, Song Ma suture; 4, Truong Son suture; 5, Luang Prabang suture; 6, Jinghong suture; 7, Nan suture; 8, Changling-Menglian suture; 9, Inthanon suture. Major Indosinian granitic plutons and their isotopic ages: WWT, Wawutang; BM, Baimashan; GDM, Guandimiao; YM, Yangmingshan; ZG, Zhuguangshan; F-H, Fucheng-Hongshan; XT, Xiaotao; LYB, Longyuanba; GK, Guikeng; GD, Guidong; WLT, Wuliting; DR, Darongshan; WZS, Wuzhishan. (b) Simplified geological map of Hainan Island (modified after Guangdong BGMR, 1988) showing sampling locations. In panel (b), the ages of Indosinian granites on Hainan Island are from Xie *et al*. (2005), Li *et al*. (2006), Mao *et al*. (2013), Yan *et al*. (2017) and this study. The ^{40}Ar-^{39}Ar ages of the high-strain shear zones are from Zhang *et al*. (2011). (c) A geologic section of (b). T_1, early Triassic; T_3, late Triassic.

Many researchers have attempted to solve the location problem of the paleo-Tethys suture zones on Hainan Island. Yang *et al*. (1989) divided Hainan Island into a northern Qiongzhong terrane and a southern Yaxian terrane (*i.e*., Sanya block) based on stratigraphy and paleontology, which are separated by the east-west-trending Jiushuo-Lingshui fault (Fig.1b). The suture zone is considered to have formed in the Cretaceous (Yang *et al*., 1989). Li *et al*. (2002) proposed that the Bangxi (*i.e*., Changjiang) and Chenxing (*i.e*., Tunchang) metabasites with amphibolite-facies metamorphism from the central Hainan Island are similar to mid-ocean ridge basalts (MORB), on which the Sm-Nd isochron yielded a crystallization age of 333±12 Myr. The South China continent (*i.e*., the north part of Hainan Island) and Indochina block (including the south-central part of Hainan Island) are bounded by the Changjiang-Qionghai fault (Li *et al*., 2002; Fig.1b). Xu *et al*. (2008) suggested that the NE-SW-trending Baisha fault should mark the paleo-Tethys suture zone derived from the collision of an early Paleozoic intraoceanic arc with the South China continent (Fig.1b). The Tunchang metabasites are relics of an intraoceanic island arc rather than N-MORB-type rocks in a subduction setting, and the Bangxi metabasites more likely formed in an extensional back-arc basin (Xu *et al*., 2008). The Bangxi metabasites have a protolith age of 269±4 Myr, recording the timing of expansion of an epicontinental back-arc basin due to the early Carboniferous–early Permian subduction of the paleo-Tethys (Xu *et al*., 2007). Liu *et al*. (2006, 2011) believed that there was a paleo-Tethys oceanic basin (*i.e*., Qiongnan oceanic basin) between the Qiongzhong block and Sanya block. After the mid-Triassic, the Qiongnan oceanic basin was completely subducted, resulting in the collision and suturing of the two blocks, which formed the 'Qiongnan suture zone', represented by the Jiusuo-Lingshui fault zone (Xie *et al*., 2005; Liu *et al*., 2006, 2011; Tang, 2010).

As outcrops of paleo-Tethys-related ophiolites have not been found, the eastward extension of the Song Ma suture on Hainan Island is still disputed. A series of WNW-trending shear zones with 258–240 Myr foliated granites have been identified in the Ailaoshan, Song Ma and Truong Son zones (Lepvrier *et al*., 1997; Lan *et al*., 2000; Carter *et al*., 2001). These ductile shear zones accompanied by the contemporary foliated granites and gneisses were thought to represent responses to the closure of the paleo-Tethys (Metcalfe, 1996, 2017; Carter *et al*., 2001; Wang *et al*., 2007). Recently, the NE trending high-strain shear zones (Shen *et al*., 2016; Wang *et al*., 2018) and foliated granites (this study) closed to the Jiusuo-Lingshui fault have been discovered on the southern Hainan Island (Fig.1b). These structures might play important roles in deciphering the Indochina–South China continent collisional tectonic evolution. In this paper, we present our new results on the kinematics and geochronology of two shear zones (*i.e*., the Xiaomei shear zone and the Mangsan shear zone) (Fig.1b). A synthesis of these data provides an important constraint on the Triassic amalgamation of the Indochina with the South China continent and the tectonic evolution of the paleo-Tethys on the Hainan Island.

2 Geological Setting

Hainan Island is a continental island separated from the South China mainland by the Qiongzhou Strait (Li *et al*., 2002; Zhang *et al*., 2011). The Mesoproterozoic basement of Hainan Island is composed of high greenschist- to amphibolite-facies granitic gneisses (1.43 Ga) and minor metasediments and metavolcanics of the Baoban Group and greenschist-facies metasedimentary and metavolcanic rocks (1.44 1.43 Ga) of the Shilu Group (Guangdong BGMR, 1988; Li *et al*., 2002; Yan *et al*., 2017). The Cambrian and Ordovician strata are predominantly composed of shale, sandstone, siltstone and slate with limestone interlayers (Wang *et al*., 1991; Yao and Huang, 1999; Zeng *et al*., 2003, 2004; Zhang *et al*., 2011). The upper Paleozoic successions are characterized by Carboniferous slate, lower Permian limestone and middle Permian sandstone (Zhang *et al*., 2011), belonging to marine sediments (Liu *et al*., 2006). These rocks predominantly crop out to the north of the Jiusuo-Lingshui fault (*i.e*., Qiongzhong block) (Hu *et al*., 2001; Liu *et al*., 2006, 2011; Long *et al*., 2007). However, the area to the south of the Jiusuo-Lingshui fault (Sanya block) has been uplifted and denuded and thus lacks sedimentary records from the late Ordovician to middle Permian (Liu *et al*., 2006). At the end of the Permian, the Indosinian orogeny ended the marine sedimentation on the Qiongzhong block, followed by the collision between the Sanya and Qiongzhong blocks (Xie *et al*., 2005; Liu *et al*., 2006, 2011, 2017; Tang, 2010; Shen *et al*., 2016; Wang *et al*., 2018). Lower-middle Triassic coarse clastic rocks (molasse formation) occur only in the Anding and Qionghai areas in the central and northern island (Zhang *et al*., 2011) and are products of the Indosinian orogeny (Tang, 2010). The lower Cretaceous Lumuwan Formation consists of terrestrial siliciclastics. The Cenozoic strata have large variations in thickness, exceeding 3000 m in some depressional basins.

Hainan Island can be divided into several tectonic blocks. Two major tectonic belts are developed on Hainan Island. One is an E-W-trending belt, and the other is a NNE-trending belt (Zhang *et al*., 2011; Yan *et al*., 2017). Four large E-W-trending faults, the Wangwu-Wenjiao, Changjiang-Qionghai, Jianfeng-Diaoluo and Jiusuo-Lingshui faults, occur from north to south, based on aeromagnetic data (Guangdong BGMR, 1988; Zhang *et al*., 2011; Yan *et al*., 2017; Fig.1b). The NE-SW-trending Baisha fault divides Hainan Island into two parts, namely, the northwest Hainan block and southeast Hainan block (Li *et al*., 2002). These faults constitute important tectonic boundaries (Tang, 2010). Granites crop out extensively on Hainan Island and occupy 37% of the island's land area (Wang *et al*., 1991) (Fig.1b). Granites have multiple periods of intrusive activity, among which Indosinian and Yanshanian granites are the most widely distributed (Guangdong BGMR, 1988; Zhang *et al*., 2011). The Indosinian granite was formed in the Triassic, related to the collision during the Indosinian orogeny (Ge, 2003; Xie *et al*., 2005; Li *et al*., 2006; Liu *et al*., 2006).

3 Sampling and Methods

3.1 Sampling

The Mangsan shear zone (18°30′56″N, 109°46′05″E) and Xiaomei shear zone (18°39′41″N, 109°56′53″E) are located in the southeastern part of Hainan Island and closed to the Jiusuo-Lingshui fault (Fig.1b). In this study, we collected three syntectonic granites (XM01, XM06, and XM 10), two granites (XM04 and XM05), and three granitic gneisses (XM02, XM03, and XM07) from the Xiaomei shear zone (Fig.1c) and four gneissic granites (MS24, MS25, MS26, and MS27) from the Mangsan shear zone (Fig.1b). The granite samples (XM04 and XM05) were collected from the pluton emplaced into the syntectonic granites (XM06, and XM10) along the faults in the outcrop.

Syntectonic granites (XM01, XM06, and XM10) contain large plagioclase (50%), potassium-feldspar (25%) and quartz (20%), and minor biotite (3%) and hornblende (2%). Two granite samples (XM04 and XM05) comprise mainly plagioclase (55%), quartz (25%), potassium-feldspar (16%) and minor biotite (3%) and hornblende (1%). The granitic gneisses (XM02, XM03, and XM07) are typically pale gray in color, containing plagioclase (50%), K-feldspar (25%), quartz (15%), biotite (5%), and hornblende (5%). The gneissic granites (MS24, MS25, MS26, and MS27) are typically pale gray to white in color and contain plagioclase (50%), K-feldspar (20%), quartz (20%), biotite (5%), and hornblende (5%) with gneissic texture (Fig.2d).

3.2 Scanning Electron Microscope (SEM) Images

The syntectonic granite sample (XM01), granite sample (XM04) and gneissic granite (MS24) were analyzed with a NOVA NANOSEM 450 scanning electron microscope (SEM) at the State Key Laboratory of Nuclear Resources and Environment, East China University of Technology. Before the experiment, the granitic gneisses were cut into cubes of approximately 1 cm^3. Then, the samples were wrapped with conductive glue on the sample preparation stage, exposing the observed surface，which should be parallel to the lineation and perpendicular to the foliation. Subsequently, the gold-plating instrument of model Q150RS was used to spray gold onto the surfaces of the samples with a duration about 100 s or 150 s.

3.3 Zircon U-Pb Dating Method

Zircons were separated from crushed rock samples using standard gravimetric and magnetic separation techniques and later handpicked under a binocular microscope. Around 200 zircon grains from each sample were mounted randomly on epoxy resin. For each grain the analytical spots were chosen based on careful examination of cathodoluminescence (CL) images which were used to identify the internal features of zircons. LA-ICP-MS (laser ablation inductively coupled plasma mass spectrometry) dating of zircons from 9 samples was performed at the Key Laboratory of Mineralogy and Metallogeny, Guangzhou Institute of Geochemistry, Chinese Academy of Sciences. U, Th, and Pb concentrations were calibrated using NIST 610 as the reference material. External standard 91500 (1062.4 ± 0.4 Myr) (Wiedenbeck *et al*., 1995) and Plesco-vice zircon (337.13 ± 0.37 Myr) (Sláma *et al*., 2008) were used for calibration. Isotope ratios were calculated using ICPMS Data Cal 10.7 (Liu *et al*., 2010). We used $^{206}Pb/^{238}U$ ages for zircon grains younger than 1000 Myr and $^{207}Pb/^{206}Pb$ ages for those older than 1000 Myr. The weighted mean ages were calculated for the granite samples. Age histograms with probability for the rocks were created with Isoplot 4.11 (Ludwig, 2003).

3.4 Major and Trace Element Geochemical Analysis

Sample preparation and whole-rock analysis were carried out at ALS Laboratory Group (Guangzhou, China). Samples were fused with lithium metaborate-lithium tetraborate flux, including an oxidizing agent (lithium nitrate), and then poured into a platinum mould. Fusion disks and powder pellets for major element analyses were measured using a PAN analytical Axios Max XRF (Almelo, The Netherlands). The precision for major elements is better than 5%. For the trace elements of the samples, the resultant solutions were determined using an ICP-MS (Agilent 7700×ICP-MS, USA) at the ALS Group (Guangzhou, China). The precision for trace elements is better than 5%–10%.

4 Results

4.1 Sinistral Shear Stress Along the Xiaomei Shear Zone and Mangsan Shear Zone

The NE-trending Xiaomei shear zone extends more than 4 km with a width of 100–120 m. It comprises a series of individual shear zones (50–80 m wide and hundreds of meters long) and crops out discontinuously as tectonic slices along the river. The shear zones are characterized by the development of syntectonic granites and granitic gneisses with gneissic texture. Felsic minerals such as feldspar and quartz are elongated to form lineations (Fig.2a). The a-lineations are developed with NNE (18°) pitch direction at the pitch angle of approximately 35°. Dynamic recrystallization of feldspar and quartz is common in the syntectonic granites and granitic gneisses. The kinematic indicators observed in the Xiaomei shear zone include outcrop-scale quartz veins, asymmetric porphyroblasts with attenuated tails (Fig.2a), structural lenses (Fig.2b) and S-shaped asymmetrical folds, suggesting predominant sinistral shear stress.

The microscopic structures reflect the same characteristics as the macroscopic structures (Cao and Wang, 2004). These features include microscopic S-C fabrics, mica flakes and asymmetric porphyroblasts (Figs.3a, b), indicating a sinistral shear component. The feldspar and quartz display distinct undulose extinction.

Scanning electron microscopy reveals more detailed deformation structures in the syntectonic granite (XM01). The kinks and folds are widespread in the biotite of the

syntectonic granite (XM01) (Figs.4a, b, c, d). Biotite shows kinked geometry, presenting asymmetric folds (Fig.4a), which is consistent with sinistral shearing observed from the macroscopic outcrops and Polarized microscope. In addition to the kinks, symmetrical folds (Fig.4b), tight folds (Fig.4c) and Jura-type folds (Fig.4d) can be seen in the SEM images of the syntectonic granite (XM01). Tight folds that emerge in the biotite generally are formed under strong compression and Jura-type folds indicate constrained strain.

Fig.2 Field photographs of the Xiaomei shear zone and Mangsan shear zone. (a), asymmetric porphyroblasts with attenuated tails in syntectonic granite (XM01) from the Xiaomei shear zone indicate sinistral shearing; (b), Felsic lenses in granitic gneiss (XM02) from the Xiaomei shear zone indicate strong shearing; (c), The granite sample (XM04) without any shearing in the Xiaomei area; (d), Asymmetric porphyroblasts with attenuated tails in gneissic granite (MS24) from the Mangsan shear zone indicate sinistral shearing.

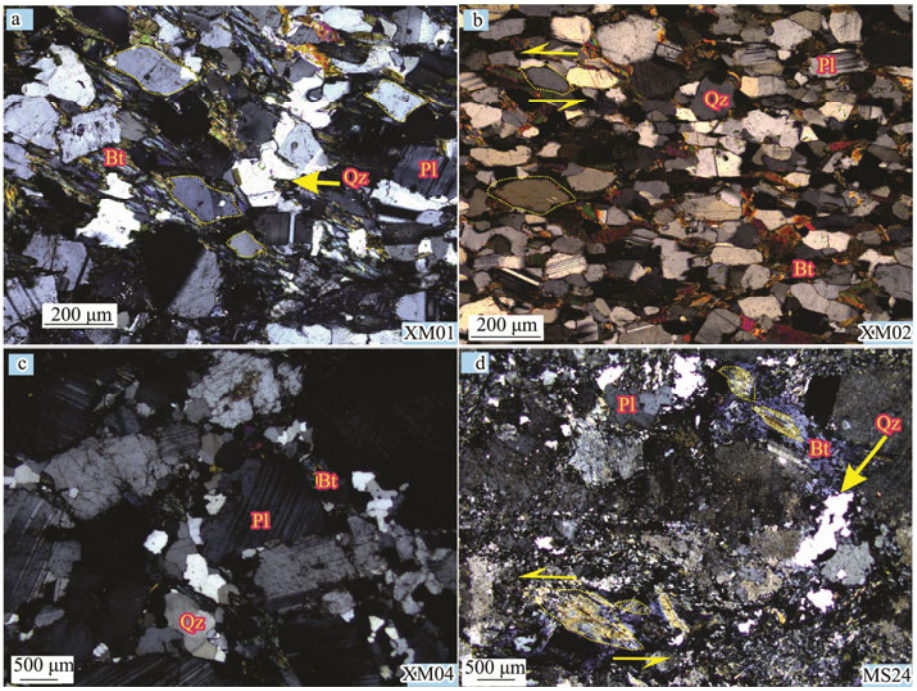

Fig.3 Photomicrographs of rock samples. (a), Asymmetric porphyroblasts with recrystallized tails in the syntectonic granite (XM01); (b), Asymmetric porphyroblasts in the granitic gneiss (XM02); (c), Photomicrograph of the granite sample (XM04) without any shearing; (d), The microscopic mica flake shows sinistral shearing deformation in the Mangsan shear zone. Qz, quartz; BT, biotite; Pl, plagioclase.

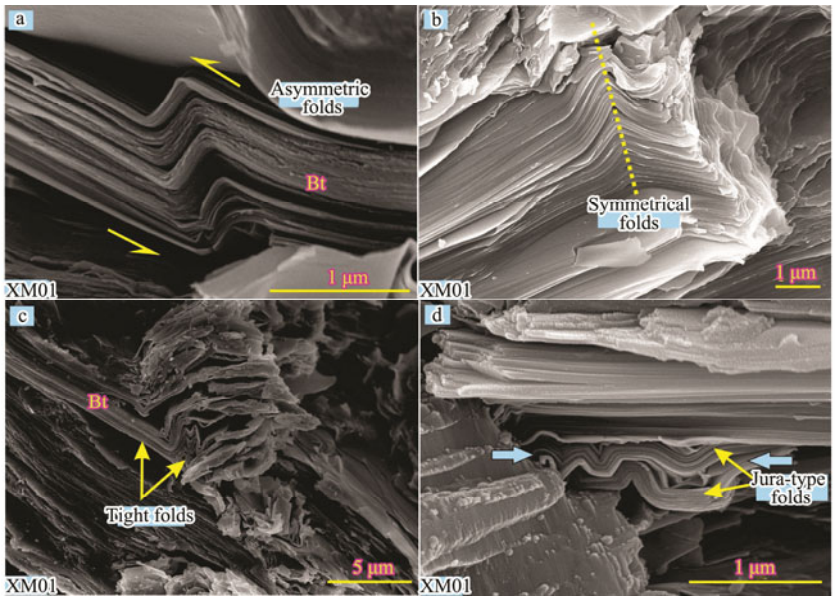

Fig.4 Scanning electron microscopy (SEM) images of syntectonic granite (XM01) viewed on the $X-Z$ section. (a) Kinks showed sinistral shearing deformation. (b–d) Symmetrical folds, tight folds, and Jura-type folds indicated strong compression in the Xiaomei shear zone. BT, biotite.

In general, the different scales of deformation features reflect sinistral shearing along the Xiaomei shear zone. The structural elements generally point to a ductile shear zone.

The NNE-trending Mangsan shear zone extends more than 2 km. It crops out discontinuously as tectonic slices in the northern part of the Mangsan reservoir. The shear zone is characterized by the development of gneissic granites, which are composed predominantly of biotite granite and granodiorite. The gneissic foliations can be defined by parallel feldspar phenocrysts and biotite flakes (Fig.2d). Felsic minerals such as feldspar and quartz are elongated to form lineations. The kinematic indicators observed in the Mangsan shear zone include outcrop-scale asymmetric porphyroblasts with attenuated tails (Fig.2d), microscopic mica flakes (Fig.3d), indicating the occurrence of top-to-the-NE shearing. Shearing planes without folds are developed in the gneissic granite (MS24) observed through SEM (Figs.5c, d). Stress minerals (*i.e.*, biotite, plagioclase) mostly slide along the shearing plane, and the formation of the Micron-sized grains is relatively widespread (Figs.5c, d).

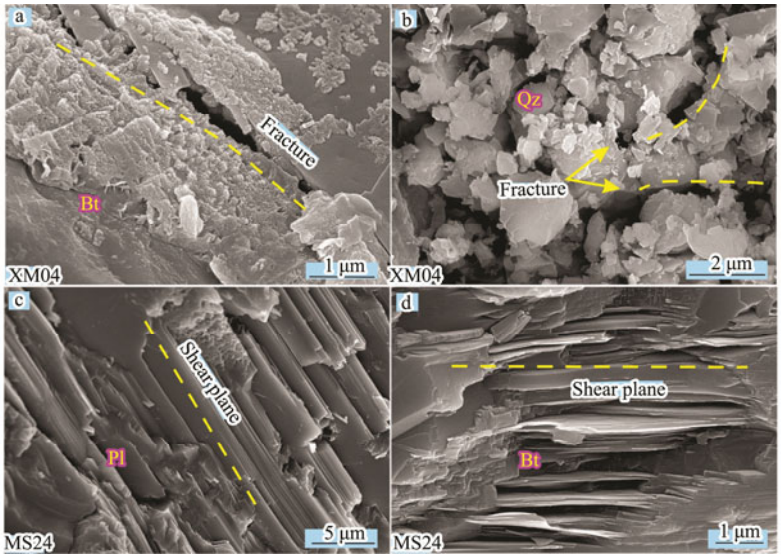

Fig.5 (a–b) Scanning electron microscopy (SEM) images of fractures in the granite sample (XM04). (c–d) Shearing lineations without folds in the Mangsan gneissic granite (MS24). Bt, biotite; Qz, quartz; Pl, plagioclase.

Granite sample (XM04) crops out in the Xiaomei area without any shearing (Fig.2c). The undeformed plagioclase and quartz are observed in the polarized microscope (Fig.3c). Scanning electron microscopy reveals brittle fracture structures widely distributed in the granite sample (XM04) (Figs.5a, b). Compared with the granitic gneiss

(XM02) and syntectonic granite (XM01), the grain size and the proportions of plagioclase and quartz gradually increase, whereas the amounts of biotite and hornblende decrease (Fig.3c).

The agglomerated nanoparticles are observed in the SEM images of the syntectonic granite (XM01) (Figs.6c, d). These agglomerated nanoparticles are formed under the high temperatures (>500℃) and high-pressure condition (Cai *et al*., 2019). The agglomerated nanoparticles exhibit various shapes within the Xiaomei ductile shear zone, including 'strawberry' shape (Fig.6c) and 'flower' shape (Fig.6d), which is similar to the nano-aggregates developed in the Ailaoshan ductile shear zone (Cai *et al*., 2019).

4.2 LA-ICP-MS Zircon U-Pb Ages

4.2.1 Middle Permian gneissic granites

Four samples (MS24, MS25, MS26, and MS27) were dated by using LA-ICP-MS. Zircon grains extracted from the samples are typically colorless or transparent and range in length from 100 μm to 400 μm with aspect ratio of 1:1 to 4:1 (Figs.7a, b, c, d). Their shapes range from euhedral to subhedral, and most grains show oscillatory zoning. The majority of the zircons have Th/U ratios that vary from 0.21 to 0.51 (0.21–0.32 for MS24, 0.17–0.43 for MS25, 0.16–0.36 for MS26 and 0.21–0.51 for MS27) and cluster within 0.2–0.5 (not shown), indicating a magmatic origin (Hoskin and Black, 2000; Belousova *et al*., 2002).

Samples MS24, MS25, MS26, and MS27 of gneissic granites from the Mangsan shear zone yield the weighted mean $^{206}Pb/^{238}U$ ages of 262.2±1.2 Myr (MSWD=0.14, n=19), 264.0±1.2 Myr (MSWD=0.24, n=19), 261.8±1.1 Myr (MSWD=0.057, n=22) and 264.0±1.1 Myr (MSWD=0.15, n=21), respectively (Figs.7a, b, c, d). The ages of the four samples in the Mangsan shear zone range from 264 to 261 Myr.

4.2.2 Early Triassic syntectonic granites

Three samples (XM01, XM06, and XM10) (Fig.1c) were dated by using LA-ICP-MS. Zircon grains extracted from the samples are typically colorless or transparent and range in length from 100 μm to 300 μm with aspect ratios of 1:1 to 3:1 (Figs.8a, b, c). Their shapes range from euhedral to subhedral, and most grains show oscillatory zoning. The majority of the zircons have Th/U ratios that vary from 0.2 to 0.7 (0.08–0.52 for XM01, 0.11–0.28 for XM06, and 0.09–0.70 for XM10) and cluster within 0.2–0.5 (not shown), indicating a magmatic origin (Hoskin and Black, 2000; Belousova *et al*., 2002).

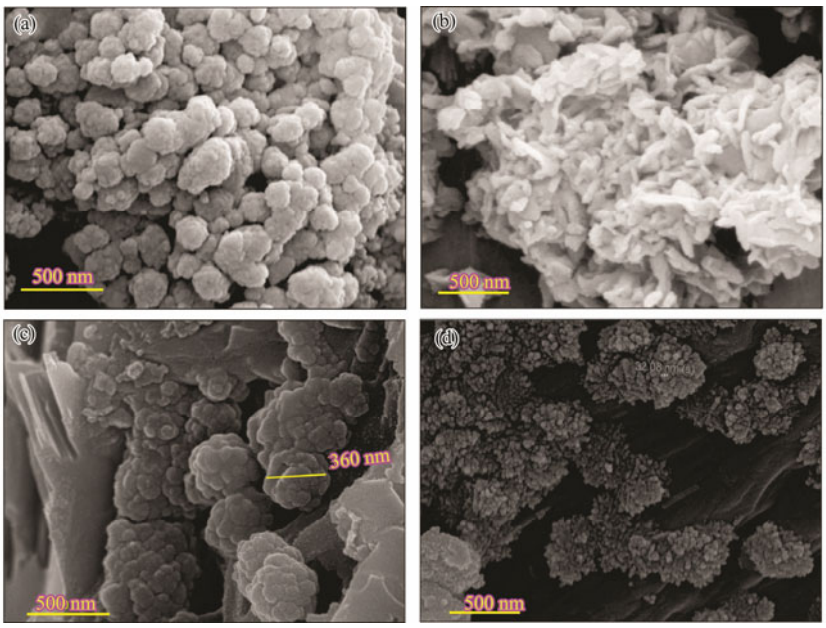

Fig.6 (a–b) Scanning electron microscopy (SEM) images of the 'strawberry' shape (a) and 'flower' shape (b) agglomerated nanoparticles in the granite sample from Ailaoshan ductile shear zone (Cai *et al*., 2019). (c–d) Scanning electron microscopy (SEM) images of the 'strawberry' shape (c) and 'flower' shape (d) agglomerated nanoparticles in the syntectonic granite (XM01) from Xaiomei ductile shear zone.

Zircons from samples XM01, XM06, and XM10 of syntectonic granites in the Xiaomei area yield the weighted mean $^{206}Pb/^{238}U$ ages of 251±1.3 Myr (MSWD=0.078, n=19), 252±1.2 Myr (MSWD=0.22, n=20) and 252.8±1.4 Myr (MSWD=0.56, n=18), respectively (Figs.8a, b, c). In general, the ages of the three samples from the Xiaomei shear zone, ranging from 252 to 251 Myr are interpreted to represent the shearing age for the NNE-trending Xiaomei shear zone.

4.2.3 Late Triassic granite

The granitic rocks were emplaced along tension fractures in the Xiaomei shear zone, and did not undergo ductile shear deformation. Two samples (XM04 and XM05) (Fig.1c) were dated using LA-ICP-MS. Zircon grains are typically colorless and range in length from 100 μm to 300 μm with aspect ratios of 1:1 to 3:1 (Figs.9a, b). Their shapes range from subrounded to angular, with obvious

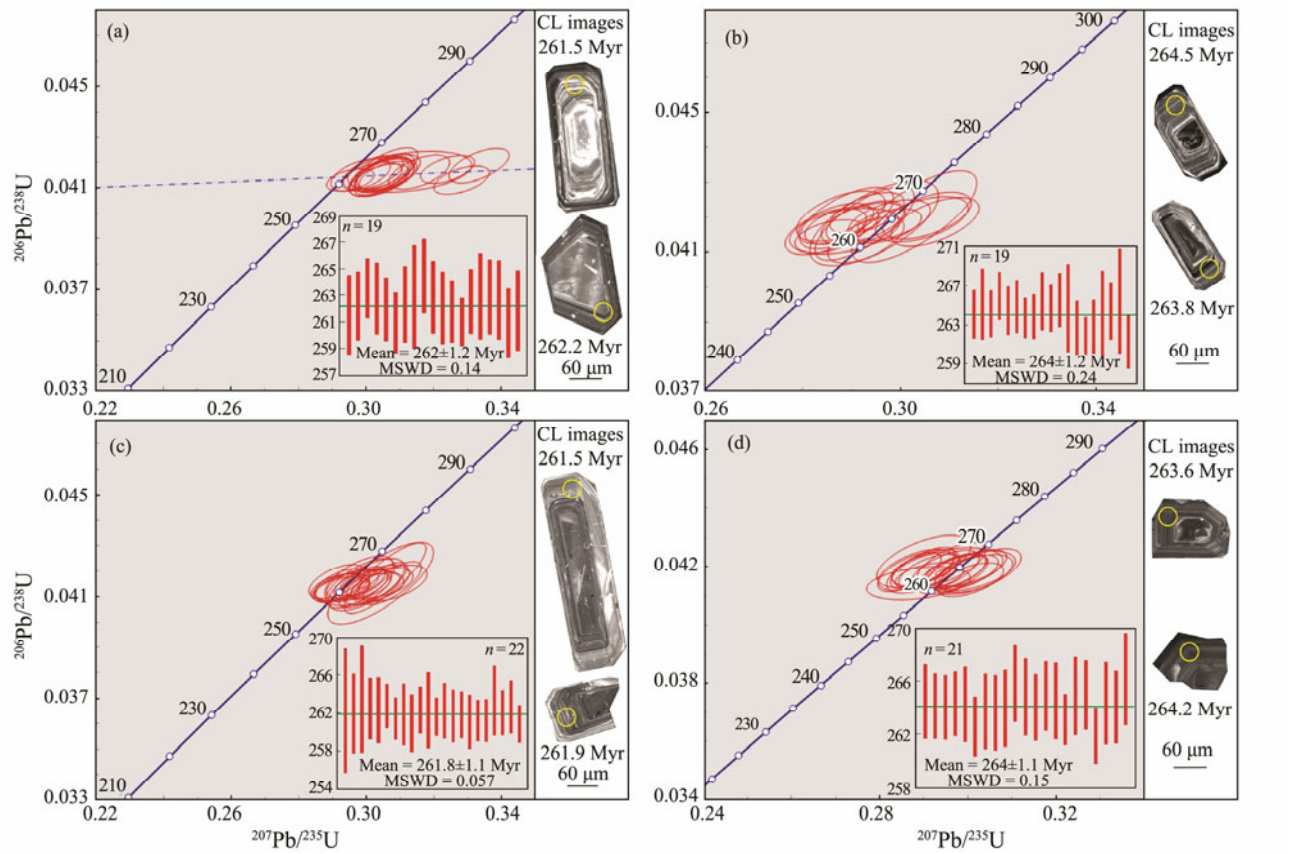

Fig.7 LA-ICP-MS zircon U-Pb concordia age diagram for gneissic granites from the Mangsan area on southern Hainan Island. (a), (b), (c), and (d) represent samples MS24, MS25, MS26, and MS27, respectively.

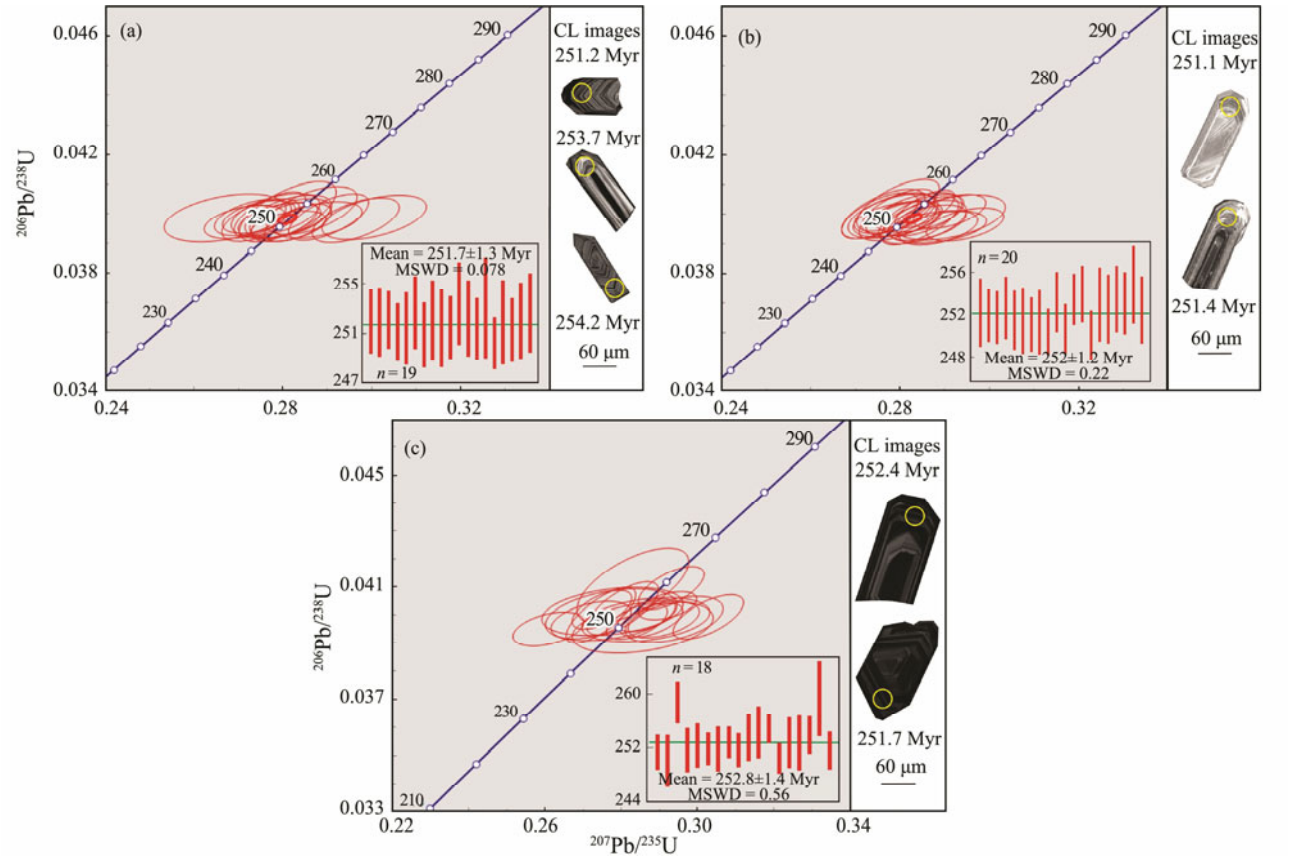

Fig.8 LA-ICP-MS zircon U-Pb concordia age diagram for syntectonic granites from the Xiaomei area on southern Hainan Island. (a), (b), and (c) represent samples XM01, XM06, and XM10, respectively.

oscillatory zoning, indicating a typical igneous origin. The Th/U ratios of all analyzed zircons for two samples vary from 0.44 to 1.06 (0.47–1.06 for XM04 and 0.44–0.99 for XM05), which is consistent with their magmatic origin (Hoskin and Black, 2000; Belousova *et al.*, 2002). A weighted mean $^{206}Pb/^{238}U$ age of 232.9±1.2 Myr (MSWD =0.41, n=23) is calculated for sample XM04 (Fig.9a). Zircons from sample XM05 in the Xiaomei area yield the weighted mean $^{206}Pb/^{238}U$ age of 235.3±1.2 Myr (MSWD =0.035, n=22) (Fig.9b).

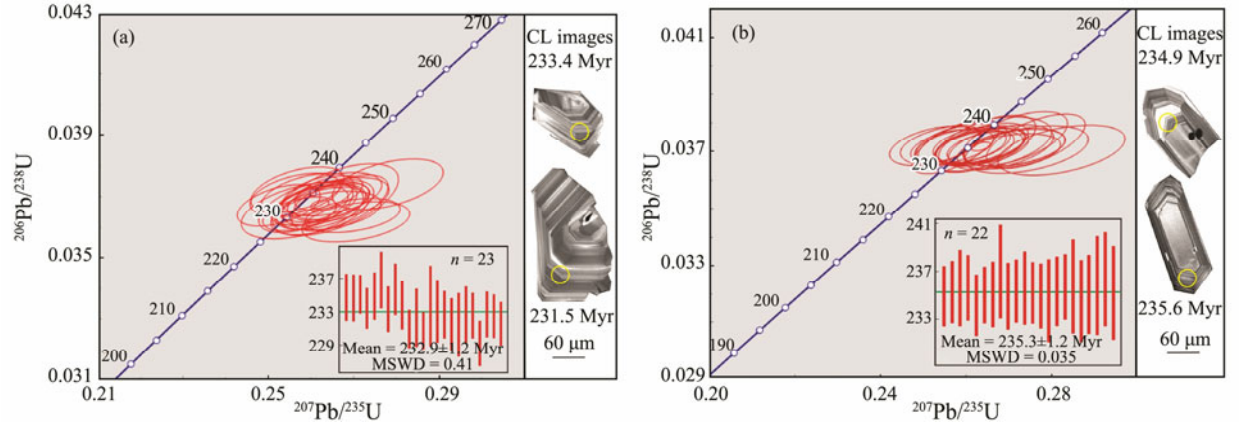

Fig.9 LA-ICP-MS zircon U-Pb concordia age diagram for the granites from the Xiaomei area in southern Hainan Island. (a) and (b) represent samples XM04 and XM05, respectively.

4.3 Major and Trace Element Geochemical Analysis

Major and trace element compositions are listed in the Tables 1 and 2. The granite samples from southern Hainan Island have high SiO_2 values, ranging from 67.19 wt% to 76.35 wt%. In the TAS ((Na_2O+K_2O) *vs.* SiO_2) diagram (Fig.10a) (Middlemost, 1994), the samples plot in the fields of granodiorites, granites, and quartz monzonites, belonging to the subalkaline series (Fig.10a). The K_2O contents of the granites range from 3.02 wt% to 6.88 wt%. In the K_2O *vs.* SiO_2 diagram (Fig.10b) (Peccerillo and Taylor, 1976), the bulk of the samples plot in the fields of the high-K rock series, and a small number of the samples plot within the fields for the shoshonite series (sample XM01), or the middle-K series (sample MS25). In the A/NK *vs.* A/CNK diagram ($Al_2O_3/(Na_2O+K_2O)$ *vs.* $Al_2O_3/(CaO+Na_2O+K_2O)$) (Fig.10c) (Maniar and Piccoli, 1989), the A/NK contents of the samples mainly range from 1.52 wt% to 1.98 wt%. All the samples plot in the peraluminous fields (A/CNK > 1.1) (White and Chappell, 1983).

Table 1 Major element composition of the granites from the Hainan Island

Sample	SiO_2	K_2O	Al_2O_3	Na_2O	CaO	MgO	TiO_2	P_2O_5	FeO*	A/CNK
XM01	70.48	6.88	14.60	2.41	1.41	0.51	0.28	0.09	2.44	1.36
XM04	74.35	5.90	13.15	2.51	0.70	0.15	0.13	0.02	1.88	1.44
XM05	74.89	6.17	13.28	2.58	0.50	0.12	0.10	0.01	1.54	1.44
XM06	75.25	6.38	13.18	2.01	1.14	0.12	0.06	0.03	1.43	1.38
XM10	69.29	6.14	14.19	2.18	1.63	0.67	0.40	0.13	3.54	1.43
MS24	76.35	4.91	12.73	3.38	0.17	0.08	0.08	0.02	1.72	1.50
MS25	68.92	3.02	15.22	4.67	1.28	0.82	0.48	0.14	3.98	1.70
MS26	67.19	4.17	15.79	4.24	2.44	0.75	0.44	0.13	4.22	1.46

Primitive mantle-normalized trace element spidergrams and chondrite-normalized REE distribution patterns for these granites are shown in tne Figs.11a and 11b, respectively. Most samples show relative enrichment in light rare earth elements (LREE), with high $(La/Yb)_N$ ratios of 5.2–125.1 and strongly negative Eu anomalies (δEu = 0.20–0.44) except for the sample XM06. The negative Eu anomalies of samples XM04 and XM05 are 0.20 and 0.29, respectively, which are consistent with the Eu anomalies (<0.3) of alkaline granite. According to Green and Hunt (1980), the obvious negative Eu anomalies show the fractionation of plagioclase. The high $(La/Yb)_N$ ratios (>1) and negative Eu anomalies of granitic rocks indicate that they experienced strong fractional crystallization (*e.g.*, plagioclase). In the primitive mantle-normalized trace element spidergrams, all studied samples show distinct negative anomalies in Ba, Nb, Ta, Ce, Sr, P and Ti and positive anomalies in Rb, Pb, Th, and U (Fig.11a). Negative Ti anomalies are considered to be related to the fractionation of Ti-bearing phases (*e.g.*, sphene), and negative P anomalies result from the apatite separation (Yan *et al.*, 2017).

5 Discussion

Our zircon U-Pb datas for the Indosinian granites from southern Hainan Island, together with available zircon U-Pb ages of I- and A-type granites and syenites from previous researches (Xie *et al.*, 2005, 2006; Li *et al.*, 2006; Zhang *et al.*, 2011; Zhou *et al.*, 2011; Mao *et al.*, 2013; Wen *et al.*, 2013; Yan *et al.*, 2017), are summarized in a

Table 2 Trace element composition of the granites from the Hainan Island

Sample	XM01	XM04	XM05	XM06	XM10	MS24	MS25	MS26
Rb	266.00	316.00	289.00	206.00	253.00	160.00	127.50	193.50
Ba	724.00	163.00	148.50	755.00	576.00	299.00	601.00	706.00
Th	28.10	36.10	32.10	8.47	55.90	17.50	12.20	11.95
U	15.30	4.97	4.94	2.48	2.77	2.37	6.37	4.09
Nb	12.10	14.50	11.50	2.30	14.20	4.80	12.80	13.10
Ta	0.98	1.53	0.73	0.30	0.96	0.27	1.23	1.63
K	5.59	4.59	4.92	5.39	5.01	4.21	2.48	3.57
La	58.00	98.80	49.00	8.20	164.00	25.50	40.90	35.90
Ce	115.00	142.00	91.00	29.10	306.00	47.20	79.20	72.30
Pb	37.20	36.70	36.70	30.50	27.50	32.20	17.70	23.50
Pr	12.90	19.85	11.05	1.64	35.70	5.63	8.79	9.27
Sr	411.00	128.50	133.00	279.00	388.00	128.50	532.00	214.00
P	370.00	100.00	80.00	160.00	570.00	80.00	660.00	650.00
Nd	44.60	67.10	39.20	5.60	122.50	19.50	32.60	37.20
Zr	87.00	161.00	117.00	85.00	270.00	140.00	313.00	293.00
Hf	2.60	5.20	4.20	2.60	7.90	4.40	8.60	7.60
Sm	8.81	12.50	7.96	1.15	19.70	3.15	6.79	8.34
Eu	1.01	0.74	0.68	0.99	1.22	0.31	1.03	1.23
Ti	0.18	0.08	0.07	0.05	0.25	0.06	0.29	0.29
Gd	5.72	9.00	5.92	0.86	11.60	2.17	6.05	8.55
Tb	0.73	1.26	0.79	0.14	1.24	0.26	0.96	1.34
Dy	3.48	6.93	4.11	0.91	5.40	1.19	6.22	8.09
Y	15.40	37.30	20.10	4.90	20.20	5.10	32.70	48.40
Ho	0.56	1.32	0.74	0.20	0.80	0.21	1.19	1.71
Er	1.36	3.65	1.99	0.55	1.78	0.53	3.38	5.17
Tm	0.18	0.52	0.30	0.08	0.19	0.08	0.52	0.73
Yb	1.01	3.37	1.91	0.58	0.94	0.57	3.31	4.94
Lu	0.15	0.53	0.29	0.10	0.13	0.09	0.52	0.71
$(La/Yb)_N$	41.19	21.03	18.40	10.14	125.15	32.09	8.86	5.21
δEu	0.41	0.20	0.29	2.92	0.23	0.34	0.48	0.44

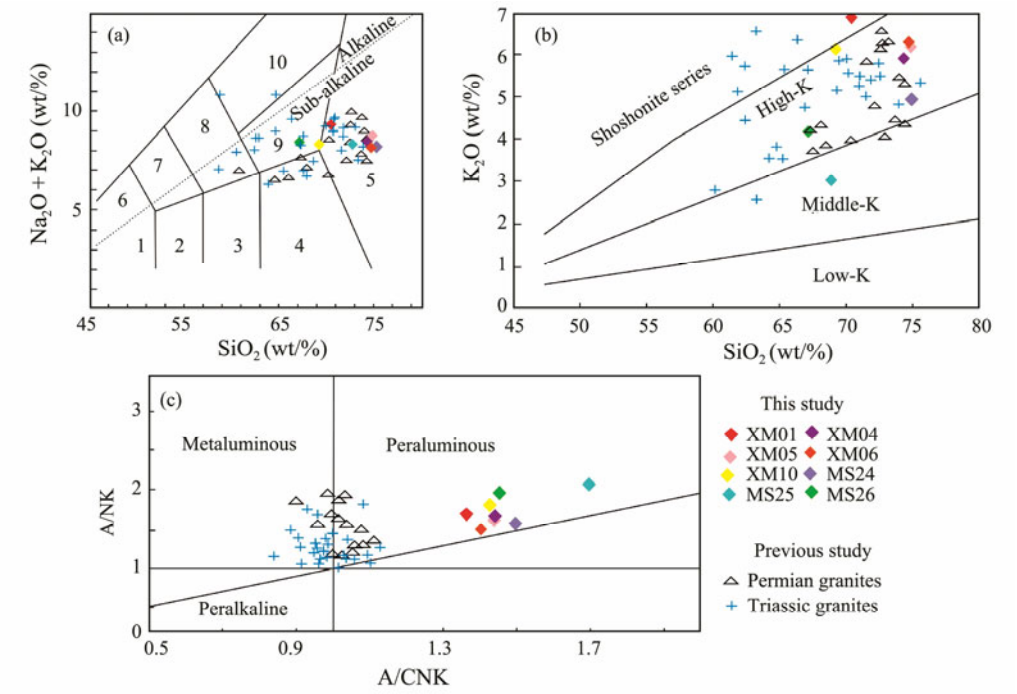

Fig.10 The rocks are classified into the different types according to (a) the SiO_2 *vs*. K_2O+Na_2O (Middlemost, 1994), (b) K_2O *vs*. SiO_2 (Peccerillo and Taylor, 1976), (c) A/NK *vs*. A/CNK (Maniar and Piccoli, 1989) diagrams. Data for the Triassic granites are from Xie *et al*. (2006) and Zhou *et al*. (2011). Data for Permian granites are from Li *et al*. (2006) and Yan *et al*. (2017). In panel (a): 1, gabbro; 2, gabbroic diorite; 3, diorite; 4, granodiorite; 5, granite; 6, monzogabbro; 7, monzodiorite; 8, monzonite; and 9, quartz monzonite.

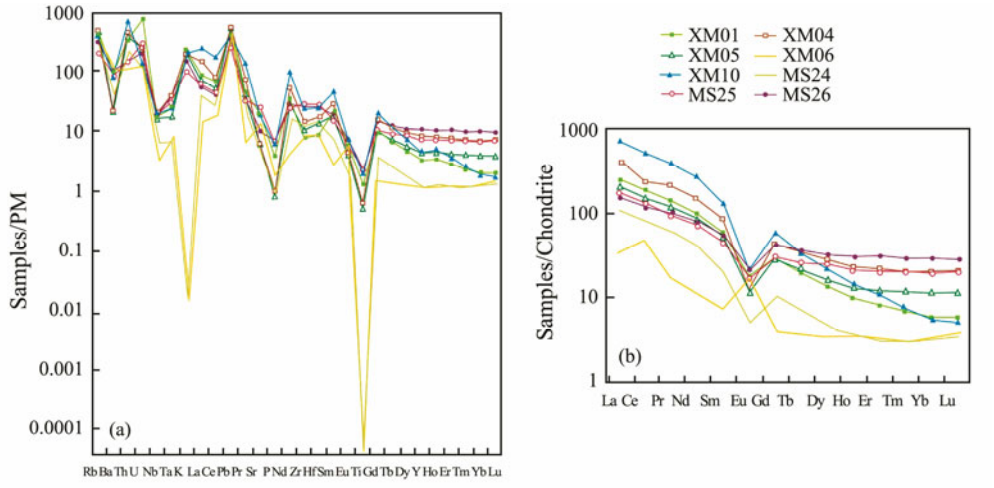

Fig.11 (a) Primitive mantle-normalized trace element spider diagram and (b) C1 chondrite-normalized rare earth element (REE) distribution pattern diagram for Permian (samples MS24, MS25 and MS26) and Triassic granitic rocks (samples XM01, XM04, XM05, XM06 and XM10) from southern Hainan Island.

histogram (Fig.12). These granites show a wide range of ages spanning 272–220 Myr, with the first igneous event at 272–260 Myr, the subordinate phase at 248–256 Myr and the third stage at 246–220 Myr. The proposed tectonic background of these granites has been described as follows.

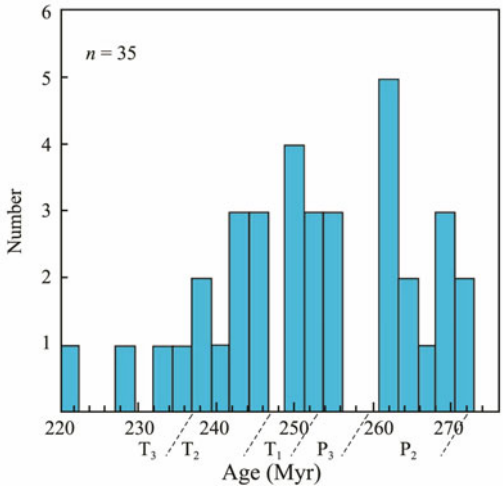

Fig.12 Zircon U-Pb age histogram for Indosinian granites on Hainan Island. In the histogram, representative ages for granitoids are from Xie *et al*. (2005, 2006), Li *et al*. (2006), Zhang *et al*. (2011), Zhou *et al*. (2011), Mao *et al*. (2013), Wen *et al*. (2013), Yan *et al*. (2017) and this study, our unpublished age data.

5.1 Middle Permian Magmatism

The middle Permian magmatism on Hainan Island is recorded by the large area of granites occurring between the Jiusuo-Lingshui and Changjiang-Qionghai faults, with ages ranging from 272 to 262 Myr (Li *et al*., 2006; Knittel *et al*., 2010; Wen *et al*., 2013; Yan *et al*., 2017). Our data demonstrate that the Mangsan gneissic granite samples (MS24, MS25, MS26, and MS27) occurred at 264–262 Myr, coinciding with a sudden change in sedimentary environments in South China during the Permian period (Li *et al*., 2006; Knittel *et al*., 2010; Wen *et al*., 2013). The middle Permian Mangsan gneissic granites are similar to the Wuzhi-shan orthogneiss in their field deformation characteristics. They are strongly foliated, defined by parallel feldspar phenocrysts and biotite flakes, with dominant NE to ENE strike directions (Li *et al*., 2006). The new major element data obtained in this study, together with data from previous studies on the middle Permian Wuzhi-shan orthogneiss (Li *et al*., 2006), show a negative relationship between SiO_2 and other major oxides (*e.g*., TiO_2, Al_2O_3, Fe_2O_3, MgO, CaO and P_2O_5), whereas Na_2O remains nearly constant. At the same time, the fractional crystallization process during the formation of the Mangsan gneissic granites is almost the same as in the Wuzhi-shan orthogneiss. Both are supported by the obvious depletions in P, Ba, Nb, and Sr and positive anomalies in Rb and Th shown in the spidergrams (Fig.10a). The REE patterns in the present study (Fig.10b) are generally similar to those of the Wuzhi-shan rocks, showing variable enrichment in light rare earth elements (LREEs), with chondrite-normalized $La_N = 151.4–552.7$, $La_N/Yb_N = 5.2–14.3$, and $Eu^*/Eu = 0.32–0.44$. In the plots of Rb *vs*. Yb+Ta (Pearce *et al*., 1984) and Nb *vs*. Y (Pearce *et al*., 1984), the middle Permian gneissic granites from the Mangsan shear zone are mainly plotted in the field of volcanic arc granites (Fig.13). Thus, we combine the Mangsan gneissic granites with the Wuzhi-shan orthogneiss in field deformation characteristics, zircon U-Pb ages, major elements, primitive mantle-normalized trace element spider diagrams, and rare earth element (REE) pattern characteristics, suggesting that they share a common source. Therefore, the Mangsan gneissic granites formed in the same tectonic setting as the Wuzhi-shan orthogneiss, and both are I-type granites (Li *et al*., 2006). These middle Permian gneissic granites with arc affinity on Hainan Island may represent the Permian arc magmatism initiated at 267–262 Myr (Li *et al*., 2006; Knittel *et al*., 2010), and their genesis may be related to the subduction of the paleo-Tethys ocean that existed between South China and the Indochina block (Lan *et al*.,

2000; Ge, 2003; Wen *et al*., 2013). Because the Jiusuo-Lingshui fault is divided according to geophysical data, the actual trending for the Jiusuo-Lingshui fault may not be east-west direction. Based on the field geological survey and analysis, we believe that the Mangsan shear zone closed to the Jiusuo-Lingshui fault is probably the true trend of the Jiusuo-Lingshui fault. The subduction direction of the paleo-Tethys ocean was NW, according to the NE sinistral shear kinematic indicators observed in the Mangsan shear zone (Fig.14a).

5.2 Late Permian and Early Triassic Magmatism

The late Permian and early Triassic granitoids mainly occur in the Qiongzhong block (Li *et al*., 2005; Xie *et al*., 2006; Yan *et al*., 2017 and this study) and the Sanya block (Xie *et al*., 2005; Yan *et al*., 2017), and the ages for these rocks range from 243 to 255 Myr (Li *et al*., 2005; Xie *et al*., 2006; Zhou *et al*., 2011; Yan *et al*., 2017 and this study). Geochemical compositions of granitic rocks can also be used to indicate their tectonic setting (Pearce *et al*., 1984). In the plots of Rb *vs*. Y+Nb (Pearce *et al*., 1984) and Nb *vs*. Y (Pearce *et al*., 1984), the early Triassic syntectonic granites in the Xiaomei area are mainly plotted in the field of syncollisional granites (Fig.13). Combining our data with the 257 Myr syncollisional granites in the Shilu and Bangxi areas of Hainan Island (Li *et al*., 2005) and the 244±7 Myr augite syenite found in the Sanya block (Xie *et al*., 2005), we determined that the collision time between the Qiongzhong block and Sanya block was approximately 257–248 Myr (Tang, 2010). In contrast, the early Indosinian granitoids in South China (T_1–T_2^1) show gneissic structures, which are interpreted as syncollisional granites under compression (Zhou *et al*., 2006). These syncollisional granites with gneissic structures are well exposed along and in the vicinity of the Song Ma suture, where the Indochina block collided with the South China block. The peak age of the collision is dated at 258 to 243 Myr (Carter *et al*., 2001). The Luoding and Fen-jienan plutons in the southwest South China block are good examples, with ^{40}Ar-^{39}Ar muscovite ages of 249.7±2.6 Myr and 255.3±3.0 Myr, respectively (Shao *et al*., 1995), which are consistent with the collision time between the Qiongzhong block and the Sanya block (257–248 Myr) (Tang, 2010). Thus, we compare the zircon U-Pb ages, deformation characteristics and nano-aggregates of the Xiaomei syntectonic granites with the floiated granites developed in the Ailaoshan ductile shear zone, suggesting that Jiusuo-Lingshui fault is likely to be the Paleo-Tethys suture on the Hainan Island. The Xiaomei syntectonic granites (252–251 Myr) on Hainan Island may represent the Indosinian collisional orogeny on Hainan Island (Fig.14b). The Micron-sized symmetric folds, tight folds, and Jura-type folds observed in the syntectonic granite (XM01) through SEM may indicate the strong compression of Indosinian collisional orogeny. The collision direction of the orogeny on Hainan Island is WNW according to the NNE sinistral shear kinematic indicators observed in the Xiaomei shear zone (Fig.14b).

5.3 Middle–Late Triassic Magmatism

The Xiaomei granite samples (XM04 and XM05) analyzed in this study yield late Triassic zircons (235–232 Myr). The chemical features of sample (XM04) include high SiO_2 (74.35%), Ga/A1 (2.6×10^{-4}), K_2O+Na_2O (8.41%), FeO* (1.88%), Zr (161 μg g^{-1}), Nb (14.5 μg g^{-1}), Ce (142 μg g^{-1}), and Y (37.3 μg g^{-1}), low CaO (0.7%), Ba (163 μg g^{-1}), and Sr (128.5 μg g^{-1}) and strongly negative Eu anomalies (δEu=0.20). The sample XM05 also exhibits high SiO_2 (74.89%), Ga/A1 (2.3×10^{-4}), K_2O+Na_2O (8.75%), FeO* (1.54%), Zr (117 μg g^{-1}), Nb (11.5 μg g^{-1}), Ce (91 μg g^{-1}), and Y (20.1 μg g^{-1}), low CaO (0.5%), Ba (148 μg g^{-1}), and Sr (133 μg g^{-1}) and strongly negative Eu anomalies (δEu=0.29). Chemical analyses reveal that both samples (XM04 and XM05) have the characteristics of A-type graites (Collins *et al*., 1982; White and Chappell, 1983; Whalen *et al*., 1987). In the plots of FeO*/MgO *vs*. 10000*Ga/A1 (Whalen *et al*., 1987) and FeO*/MgO *vs*. SiO_2 (wt%) (Eby, 1990), the Xiaomei late Triassic granites in this study are plotted in the fields of A-type granites (Figs.15a, b). The brittle fracture structures found by scanning electron microscopy in the granite sample (XM04) may suggest the local extension in the late Triassic.

Under an overall Indosinian orogeny, the occurrence of A-type granites suggests that extension had begun to de-

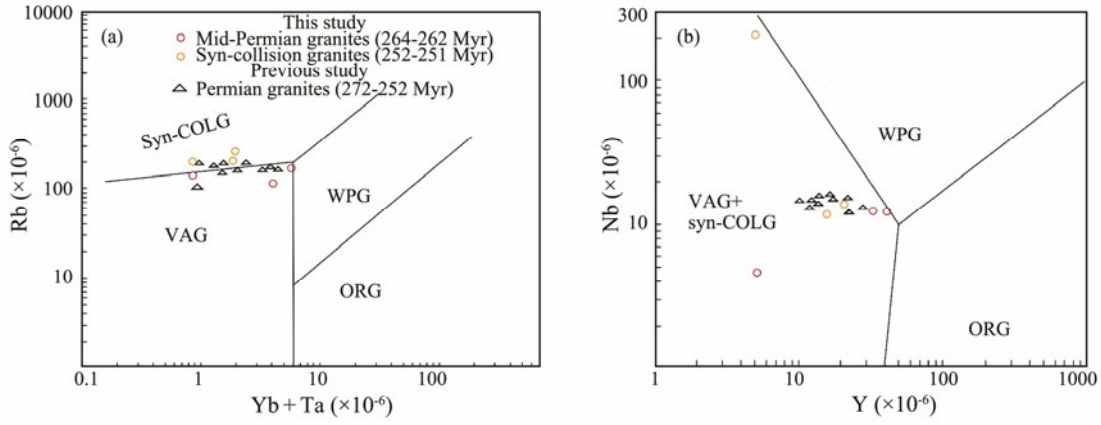

Fig.13 Trace element tectonic discriminant plots (Pearce *et al*., 1984). WPG, within-plate granite; VAG, volcanic arc granite; syn-COLG, syncollisional granite; ORG, oceanic ridge granite. The Permian granites are from Yan *et al*. (2017).

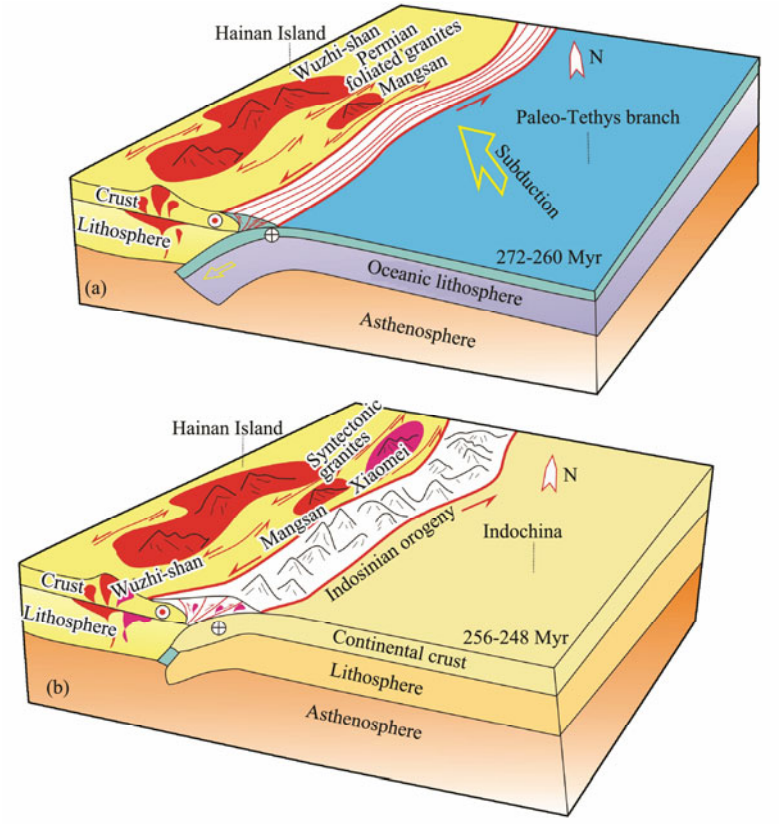

Fig.14 A cartoon showing Indosinian subduction (a) and the occurrence of syntectonic granites in the Hainan Island (b).

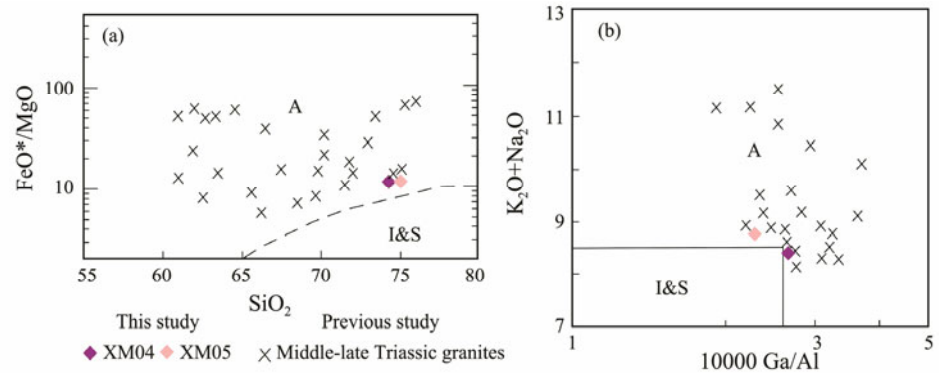

Fig.15 Geochemical plots for tectonic discriminant (Whalen *et al*., 1987; Eby, 1990). A, A-type granites; I&S, I-type granites and S-type granites.

velop (Xie *et al*., 2006; Zhou *et al*., 2011; Yan *et al*., 2017). The middle Triassic granites (243±4 Myr and 241±1 Myr) in the southeastern part of Hainan Island are A-type granites (Zhou *et al*., 2011). The middle Triassic alkali syenite (244±7 Myr) in the Sanya area has the geochemical characteristics of A-type granite (Xie *et al*., 2006). In addition, 238 Myr A-type granites, 237 Myr basic dikes, and the 231 Myr Fenjiezhou syenite were emplaced in the southeastern part of Hainan Island (Tang, 2010; Zhou *et al*., 2011), which reflects a postcollisional tectonic environment during the late Triassic (Sylvester, 1998; Bonin, 2004; Tang, 2010).

Moreover, postcollisional orogenic magmatism can be found along the western Pacific Rim of the East Asian continental margin in South Korea (Kim *et al*., 2011) and Southeast China (Sun *et al*., 2011; Mao *et al*., 2013). For example, the gabbro, monzodiorite, monzonite, syenite, and granite (232–226 Myr) in South Korea (Kim *et al*., 2011) suggest typical postcollisional orogenic magmatism (Mao *et al*., 2013). The presence of the Wengshan A-type granites (224 Myr), Jinhua alkaline A-type granitic plutons (231 Myr), and Jingju A-type granites (215 Myr) in Zhejiang Province and the Gaoxi A-type granites (215 Myr), Xiaotao A-type granites (222 Myr) and Yangfang (242 Myr) alkali syenites in Fujian Province define important extensional events in the Triassic (Sun *et al*., 2011; Mao *et al*., 2013). The ages of the Tangshi and Longtan granitic plutons in Hunan Province are 239±3 Myr and 243±3 Myr, respectively (Wang *et al*., 2005). The ages of the Wuliting pluton and Nanfucheng pluton in South Jiangxi are 238.9±

1.5 Myr (Zhang *et al*., 2004) and 239±17 Myr (Yu *et al*., 2007), respectively. The ages of the Longyuanba pluton and southern Zhuguangshan composite in North Guangdong are 241.0±1.3 Myr (Zhang *et al*., 2006) and 231–239 Myr (Deng *et al*., 2012), respectively. The SHRIMP U-Pb ages of the zircons from the Darongshan, Jiuzhou and Taima plutons in southeastern Guangxi are 233±5 Myr, 230±4 Myr and 236±4 Myr, respectively (Deng *et al*., 2004). All the geochemical characteristics of the granites listed above indicate that they were formed in a postcollisional tectonic environment (Deng *et al*., 2012). Considering these available data, the late Triassic extensional events in South Korea and Southeast China are related to subduction of the paleo-Pacific Plate beneath the East Asian continental margin (Kim *et al*., 2011; Sun *et al*., 2011; Mao *et al*., 2013). In addition, the 240.4±2.8 Myr I-type diorite, granodiorite and granite in the Dienbien complex rocks of northern Vietnam (Nguyen *et al*., 2004), the middle Triassic magmatism in western Sarawak (Breitfeld *et al*., 2017), and the 238 Myr magmatism and metamorphism in the NW Schwaner Mountains, Indonesia (Hennig *et al*., 2017), are related to the westward subduction of the paleo-Pacific Plate. The middle–late Triassic westward paleo-Pacific subduction zone associated with the collapse of the Indosinian orogen could extend from South Korea through the eastern margin of South China and Indochina to Borneo.

6 Conclusions

1) Age data for Indosinian granites from Hainan Island can be divided into three groups: middle Permian (272–260 Myr), late Permian and early Triassic (256–248 Myr), and middle–late Triassic (246–220 Myr).

2) Geochemical data, deformation characteristics, and zircon U-Pb ages for the middle Permian Mangsan gneissic granites (264–262 Myr) indicate that they are almost the same as the Wuzhi-shan orthogneiss, belonging to subalkaline I-type granites with arc affinity. The subduction direction of the paleo-Tethys ocean on Hainan Island was NW according to the NE sinistral shear observed in the Mangsan shear zone. U-Pb ages and nano-aggregates of the Xiaomei syntectonic granites presented the similarity with the Indosinian granites from Ailaoshan ductile shear zone. It's inferred that Jiusuo-Lingshui fault is likely to be the paleo-Tethys suture on the Hainan Island. Geochemical data, field occurrence, microscopic and SEM deformation characteristics for early Triassic Xiaomei syntectonic granites (252–251 Myr) suggest the Indosinian collisional orogeny on Hainan Island. The collision direction of the Indosinian collisional orogeny on Hainan Island was WNW according to the NNE sinistral shear observed in the Xiaomei shear zone. The late Triassic A-type granites (235–232 Myr) from the Xiaomei shear zone reflect a post-collisional tectonic environment on Hainan Island.

Acknowledgements

This work was supported by the National Natural Science Foundation of China (Nos. 41676048, U1701641, 41776072, and 91328205), the Key Special Project for Introduced Talents Team of Southern Marine Science and Engineering Guangdong Laboratory (Guangzhou) (No. GML 2019ZD0205), and the Innovation Academy of South China Sea Ecology and Environmental Engineering (No. ISEE 2020YB07).

References

Belousova, E. A., Griffin, W. L., O'Reilly, S. Y., and Fisher, N. I., 2002. Igneous zircon: Trace element composition as an indicator of source rock type. *Contributions to Mineralogy and Petrology*, **143**: 602-622.

Bonin, B., 2004. Do coeval mafic and felsic magmas in post-collisional to within-plate regimes necessarily imply two contrasting, mantle and crustal, sources? A review. *Lithos*, **78**: 1-24.

Breitfeld, H. T., Hall, R., Galin, T., Forster, M. A., and BouDagher-Fadel, M. K., 2017. A Triassic to Cretaceous Sundaland-Pacific subduction margin in West Sarawak, Borneo. *Tectonophysics*, **694**: 35-56.

Cai, Z. R., Lu, L. J., Huang, Q. T., Li, J. F., Zhong, L. F., Xiang, J. Y., Xia, B., and Liu, H. L., 2019. Formation conditions for nanoparticles in a fault zone and their role in fault sliding. *Tectonics*, **38**: 159-175.

Cao, G. Z., and Wang, Y., 2004. *Nanostructures and Nanomaterials: Synthesis, Properties and Applications*. Imperial College Press, London, 1-425.

Carter, A., Roques, D., and Bristow, C., 2001. Understanding Mesozoic accretion in Southeast Asia: Significance of Triassic thermotectonism (Indosinian orogen) in Vietnam. *Geology*, **29**: 211-214.

Chen, B., and Xie, G., 1994. Evolution of the Tethys in Yunnan and Tibet. *Journal of Southeast Asian Earth Sciences*, **9**: 349-354.

Collins, W. J., Beams, S. D., White, A. J. R., and Chappell, B. W., 1982. Nature and origin of A-type granites with particular reference to southeastern Australia. *Contributions to Mineralogy and Petrology*, **80**: 189-200.

Deng, P., Ren, J. S., Ling, H. F., Shen, W. Z., Sun, L. Q., Zhu, B., and Tan, Z. Z., 2012. SHRIMP zircon U-Pb ages and tectonic implications for Indosinian granitoids of southern Zhuguangshan granitic composite, South China. *Chinese Science Bulletin*, **57** (13): 1542-1552.

Deng, X. G., Chen, Z. G., Li, X. H., and Liu, D. Y., 2004. SHRIMP U-Pb zircon dating of the Darongshan-Shi-Wandashan granitoid belt in southeastern Guangxi, China. *Geological Review*, **50**: 426-432.

Eby, G. N., 1990. The A-type granitoids: A review of their occurrence and chemical characteristics and speculations on their petrogenesis. *Lithos*, **26**: 115-134.

Fan, W. M., Wang, Y. J., Zhang, A. M., Zhang, F. F., and Zhang, Y. Z., 2010. Permian arc–back-arc basin development along the Ailaoshan tectonic zone: Geochemical, isotopic and geochronological evidence from the Mojiang volcanic rocks, Southwest China. *Lithos*, **119**: 553-568.

Faure, M., Lin, W., Chu, Y., and Lepvrier, C., 2016. Triassic tectonics of the southern margin of the South China block. *Comptes Rendus Geoscience*, **348**: 5-14.

Faure, M., Lin, W., Schärer, U., Shu, L., Sun, Y., and Arnaud, N., 2003. Continental subduction and exhumation of UHP rocks. Structural and geochronological insights from the Dabieshan

(E. China). *Lithos*, **70**: 213-241.

Ge, X. Y., 2003. Mesozoic magmatism in Hainan Island (SE China) and its tectonic significance: Geochronology, geochemistry and Sr-Nd isotope evidences. PhD thesis. Guangzhou Institute of Geochemisty, Chinese Academy of Sciences.

Green, C. A., and Hunt, R. H., 1980. Interpretation of variation in ovarian polytene chromosomes of *Anopheles funestus* Giles, *A*. *parensis* Gillies, and *A*. *aruni*? *Genetica*, **51** (3): 187-195.

Guangdong BGMR (Bureau of Geology and Mineral Resources of Guangdong Province), 1988. Regional Geology of Guangdong Province. Geological Publishing House, Beijing, 1-602 (in Chinese).

Hennig, J., Breitfeld, H. T., Hall, R., and Nugraha, A. S., 2017. The mesozoic tectono-magmatic evolution at the paleo-Pacific subduction zone in West Borneo. *Gondwana Research*, **48**: 292-310.

Hoskin, P. W. O., and Black, L. P., 2000. Metamorphic zircon formation by solid-state recrystallization of protolith igneous zircon. *Journal of Metamorphic Geology*, **18**: 423-439.

Hu, N., Zhang, R. J., and Fang, S. N., 2001. The Devonian sequence in Hainan Island and the D-C boundary. *Hubei Geology and Mineral Resources*, **15** (4): 1-6 (in Chinese with English abstract).

Kim, S. W., Kwon, S., Hee, J. K., Yi, K., Jeong, Y. J., and Santosh, M., 2011. Geotectonic framework of Permo – Triassic magmatism within the Korean Peninsula. *Gondwana Research*, **20**: 865-899.

Knittel, U., Hung, C., Yang, T., and Iizuka, Y., 2010. Permian arc magmatism in Mindoro, the Philippines: An early Indosinian event in the Palawan Continental Terrane. *Tectonophysics*, **493**: 113-117.

Lan, C. Y., Chung, S. L., Shen, J. S., Lo, C. H., Wang, P. L., Hoa, T. T., Thanh, H. H., and Mertzman, S. A., 2000. Geochemical and Sr-Nd isotopic characteristics of granitic rocks from northern Vietnam. *Journal of Asian Earth Sciences*, **18**: 267-280.

Lepvrier, C., Maluski, H., Van Vuong, N., Roques, D., Axente, V., and Rangin, C., 1997. Indosinian NW-trending shear zones within the Truong Son belt (Vietnam): ^{40}Ar-^{39}Ar Triassic ages and Cretaceous to Cenozoic overprints. *Tectonophysics*, **283**: 105-127.

Lepvrier, C., Van Vuong, N., Maluski, H., Thi, P. T., and Vu, T. V., 2008. Indosinian tectonics in Vietnam. *Comptes Rendus Geoscience*, **340**: 94-111.

Li, S. X., Yun, Y., Fan, Y., and Zhou, J. B., 2005. Zircon U-Pb age and its geological significance for Qiongzhong pluton in Qiongzhong area, Hainan Island. *Geotectonica Metmetallogenia*, **29**: 227-233 (in Chinese with English abstract).

Li, X. H., Li, Z. X., Li, W. X., and Wang, Y., 2006. Initiation of the Indosinian orogeny in South China: Evidence for a Permian magmatic arc on Hainan Island. *The Journal of Geology*, **114**: 341-353.

Li, X. H., Zhou, H., Chung, S. L., Ding, S., Liu, Y., Lee, C. Y., Ge, W., Zhang, Y., and Zhang, R., 2002. Geochemical and Sm-Nd isotopic characteristics of metabasites from central Hainan Island, South China and their tectonic significance. *The Island Arc*, **11**: 193-205.

Lin, W., Faure, M., Monié, P., Schärer, U., Zhang, L., and Sun, Y., 2000. Tectonics of SE China, new insights from the Lushan massif (Jiangxi Province). *Tectonics*, **19**: 852-871.

Liu, H. L., Yan, P., Liu, Y. C., and Deng, H., 2006. Existence of Qiongnan suture on the north margin of the South China Sea. *Chinese Science Bulletin*, **51** (Supp II): 107-120.

Liu, H. L., Zheng, H., Wang, Y., Lin, Q., Wu, C., Zhao, M., and Du, Y., 2011. Basement of the South China Sea area: Tracing the Tethyan realm. *Acta Geologica Sinica*, **85** (3): 637-655.

Liu, H. L., Zhu, R. W., Shen, B. Y., Cai, Z. R., Liu, C. D., Zhang, X. F., Zhou, Y., Wang, Y., and Li, Y. H., 2017. First discovering of nanoscale tectonics in western of Qiongnan paleo-Tethyan suture zone in north margin of South China Sea and its geotectonic significance. *Journal of Nanoscience and Nanotechnology*, **17** (9): 6411-6422.

Liu, J. L., Tran, M., Tang, Y., Nguyen, Q. L., Tran, T. H., Wu, W., Chen, J., Zhang, Z., and Zhao, Z., 2012. Permo-Triassic granitoids in the northern part of the Truong Son belt, NW Vietnam: Geochronology, geochemistry and tectonic implications. *Gondwana Research*, **122**: 628-644.

Liu, Y. S., Gao, S., Hu, Z. C., Gao, C. G., Zong, K. Q., and Wang, D. B., 2010. Continental and oceanic crust recycling-induced melt-peridotite interactions in the trans-North China orogen: U-Pb dating, Hf isotopes and trace elements in zircons from mantle xenoliths. *Journal of Petrology*, **51** (1-2): 537-571.

Long, W. G., Tong, J. N., Zhu, Y. H., Zhou, J. B., Li, S. X., and Shi, C., 2007. Discovery of the Permian in the Danzhou-Tunchang area of Hainan Island and its geological significance. *Geology and Mineral Resources of South China*, **1**: 38-45 (in Chinese with English abstract).

Ludwig, K. R., 2003. User's manual for Isoplot 3.00: A geochronological toolkit for Microsoft Excel. Berkeley Geochronology Centre Special Publication, 1-74.

Maniar, P. D., and Piccoli, P. M., 1989. Tectonic discrimination of granitoids. *Geological Society of America Bulletin*, **101** (5): 635-643.

Mao, J. R., Ye, H. M., Liu, K., Li, Z. L., Takahashi, Y., Zhao, X. L., and Kee, W. S., 2013. The Indosinian collision-extension event between the South China Block and the Palaeo-Pacific plate: Evidence from Indosinian alkaline granitic rocks in Dashuang, eastern Zhejiang, South China. *Lithos*, **172** (4): 81-97.

Metcalfe, I., 1996. Gondwanaland dispersion, Asian accretion and evolution of eastern Tethys. *Australian Journal of Earth Sciences*, **43**: 605-623.

Metcalfe, I., 2017. Tectonic evolution of Sundaland. *Bulletin of the Geological Society of Malaysia*, **63**: 27-60.

Middlemost, E. A. K., 1994. Naming materials in the magma/igneous rock system. *Earth Science Reviews*, **37** (3-4): 215-224.

Nguyen, T. T. B., Satir, M., Siebel, W., and Chen, F. K., 2004. Granitoids in the Dalat zone, southern Vietnam: Age constraints on magmatism and regional geological implications. *International Journal Earth Science (Geological Rundsch)*, **93**: 329-340.

Pearce, J. A., Narris, N. B. W., and Tindle, A. G., 1984. Trace element discrimination diagrams for the tectonic interpretation of granitic rocks. *Journal of Petrology*, **25**: 956-983.

Peccerillo, A., and Taylor, S. R., 1976. Geochemistry of Eocene calc-alkaline volcanic rocks from the Kastamonu area, northern Turkey. *Contributions to Mineralogy and Petrology*, **58** (1): 63-81.

Shao, J. G., Peng, S. M., and Peng, S. B., 1995. ^{40}Ar/^{36}Ar-^{39}Ar/^{36}Ar isochrone dating for peripheral faults of Yunkai Massif. *Guangdong Geology*, **10**: 34-40 (in Chinese with English abstract).

Shen, B. Y., Liu, B., Liu, H. L., Zhou, Y., Liu, C. D., and Zhang, X. F., 2016. Xiaomei ductile shear zone on Hainan Island in a nanoscale perspective. *Earth Science*, **41** (9): 1489-1498 (in Chinese with English abstract).

Sláma, J., Kosler, J., Condon, D. J., Crowley, J. L., Gerdes, A., Hanchar, J. M., Horstwood, M. S. A., Morris, G. A., Nasdala, L., Norberg, N., Schaltegger, U., Schoene, B., Tubrett, M. N.,

and Whitehouse, M. J., 2008. Plesovice zircon–A new natural reference material for U-Pb and Hf isotopic microanalysis. *Chemical Geology*, **249**: 1-35.

Sun, Y., Ma, C. Q., Liu, Y. Y., and She, Z. B., 2011. Geochronological and geochemical constraints on the petrogenesis of late Triassic aluminous A-type granites in Southeast China. *Journal of Asian Earth Sciences*, **42** (6): 1117-1131.

Sylvester, P. J., 1998. Post-collisional strongly peraluminous granites. *Lithos*, **45**: 29-44.

Tang, L. M., 2010. Magmatic evidence of two tectonic extension events during the Mesozoic in Hainan Island & geodynamic implications. PhD thesis. Zhejiang University.

Wang, X. F., Ma, D. Q., and Jiang, D. H., 1991. *Geology of Hainan Island: Structural Geology*. Geological Publishing House, Beijing, 1-273 (in Chinese).

Wang, Y., Liu, H. L., Zhang, X. F., Shen, B. Y., Zhu, R. W., and Zhou, Y., 2018. Developmental stage and formation mechanism of nanoparticles in Xiaomei ductile shear zone on Hainan Island. *Earth Science*, **43** (5): 1532-1541 (in Chinese with English abstract).

Wang, Y. J., Fan, W. M., Cawood, P. A., Ji, S. C., Peng, T. P., and Chen, X. Y., 2007. Indosinian highstrain deformation for the Yunkaidashan tectonic belt, South China: Kinematics and $^{40}Ar/^{39}Ar$ geochronological constraints. *Tectonics*, **26**: TC6008.

Wang, Y. J., Fan, W. M., Liang, X. Q., Peng, T. P., and Shi, Y. R., 2005. SHRIMP zircon U-Pb geochronology of Indosinian granites in Hunan Province and its petrogenetic implications. *Chinese Science Bulletin*, **50**: 1395-1403.

Wang, Y. J., Qian, X., Cawood, P. A., Liu, H. C., Feng, Q. L., Zhao, G. C., Zhang, Y. H., He, H. Y., and Zhang, P. Z., 2017. Closure of the East Paleotethyan Ocean and amalgamation of the eastern Cimmerian and Southeast Asia continental fragments. *Earth-Science Reviews*, **186**: 195-230.

Wen, S. N., Liang, X. Q., Fan, W. M., Wang, Y. J., Chi, G. X., Liang, X. R., Zhou, Y., and Jiang, Y., 2013. Zircon U-Pb ages, Hf isotopic composition of Zhizhong granitic intrusion in Ledong area of Hainan Island and their tectonic implications. *Geotectonica et Metallogenia*, **37** (2): 294-307.

Whalen, J. B., Currie, K. L., and Chappell, B. W., 1987. A-type granites: Geochemical characteristics, discrimination and petrogenesis. *Contributions to Mineralogy and Petrology*, **95**: 407-419.

White, A. J. R., and Chappell, B. W., 1983. Granitoid types and their distribution in the Lachlan Fold Belt, southeastern Australia. *Geological Society of America Memoirs*, **159**: 21-34.

Wiedenbeck, M., Alle, P., Corfu, F., Griffin, W. L., Meier, M., Oberli, F., Quadt, A. V., Roddick, J. C., and Spiegel, W., 1995. Three natural zircon standards for U-Th-Pb, Lu-Hf, trace element and REE analyses. *Geostandards and Geoanalytical Research*, **19**: 1-23.

Xie, C. F., Zhu, J. C., Ding, S. J., Zhang, Y. M., Chen, M. L., Fu, Y. R., Fu, W. A., and Li, Z. H., 2006. Age and petrogenesis of the Jianfengling granite and its relationship to metallogenesis of the Baolun gold deposit, Hainan Island. *Acta Petrologica Sinica*, **22**: 2493-2508 (in Chinese with English abstract).

Xie, C. F., Zhu, J. C., Zhao, Z. J., Ding, S. J., Fu, T. A., Li, Z. H., Zhang, Y. M., and Yu, D. P., 2005. Zircon SHRIMP U-Pb age dating of garnet-acmite syenite: Constraints on the Hercynian-Indosinian tectonic evolution of Hainan Island. *Geological Journal of China Universities*, **11**: 47-57 (in Chinese with English abstract).

Xu, D. R., Xia, B., Bakun-Czubarow, N., Bachlinski, R., Li, P., Chen, G., and Chen, T., 2008. Geochemistry and Sr-Nd isotope systematics of metabasites in the Tunchang area, Hainan Island, South China: Implications for petrogenesis and tectonic setting. *Mineralogy and Petrology*, **92** (3): 361-391.

Xu, D. R., Xia, B., Li, P. C., Chen, G. H., Ma, C., and Zhang, Y. Q., 2007. Protolith natures and U-Pb zircon SHRIMP ages of the metabasites in Hainan Island, South China: Implications for geodynamic evolution since the late Precambrian. *Island Arc*, **16**: 575-597.

Yan, Q. S., Metcalfe, I., and Shi, X. F., 2017. U-Pb isotope geochronology and geochemistry of granites from Hainan Island (northern South China Sea margin): Constraints on late Paleozoic–Mesozoic tectonic evolution. *Gondwana Research*, **49**: 333-349.

Yang, S., Yu, Z., Guo, L., and Shi, Y., 1989. The division and palaeomagnetism of the Hainan Island and plate tectonic significance. *Journal of Nanjing University (Earth Science Edition)*, **1**: 38-46 (in Chinese with English abstract).

Yao, H. Z., and Huang, Z. X., 1999. Discovery of the Ordovician from Anning area, Hainan Island. *Geology and Mineral Resources of South China*, **1**: 14-17 (in Chinese with English abstract).

Yu, J. H., Wang, L. J., Wang, X. L., Qiu, J. S., and Zhao, L., 2007. Geochemistry and geochronology of the fucheng complex in the southeastern Jiangxi Province, China. *Acta Petrologica Sinica*, **23** (6): 1441-1456.

Zeng, Q. L., Li, Z. H., Xie, C. F., Fu, T. A., and Zhang, S., 2003. On the Silurian strata of the Hainan Island area, China. *Journal of Stratigraphy*, **27**: 267-275.

Zeng, Q. L., Li, Z. H., Xie, C. F., Fu, T. A., and Zhang, S., 2004. Discovery of late Llandoverian brachiopod *Xinanospirifer* from Hainan Island area, China with comments on the Nanhao Formation. *Acta Palaeontologica Sinica*, **43**: 86-93 (in Chinese with English abstract).

Zhang, F. F., Wang, Y. J., Chen, X. Y., Fan, W. M., Zhang, Y. H., Zhang, G. W., and Zhang, A. M., 2011. Triassic high-strain shear zones in Hainan Island (South China) and their implications on the amalgamation of the Indochina and South China Blocks: Kinematic and $^{40}Ar/^{39}Ar$ geochronological constraints. *Gondwana Research*, **19**: 910-925.

Zhang, M., Chen, P. R., Huang, G. L., Tan, Z. Z., Ling, H. F., and Chen, W. F., 2006. Single-zircon La-ICP-MS ages of the Longyuanba pluton in the eastern Nanling region and geological implication. *Acta Geologica Sinica*, **80** (7): 984-994 (in Chinese with English abstract).

Zhang, W. L., Hua, R. M., Wang, R. C., Li, H. M., and Chen, P. R., 2004. Single zircon U-Pb isotopic age of the Wuliting granite in Dajishan area of Jiangxi, and its geological implication. *Acta Geologica Sinica*, **78**: 352-358 (in Chinese with English abstract).

Zhou, X. M., Sun, T., Shen, W. Z., Shu, L. S., and Niu, Y. L., 2006. Petrogenesis of Mesozoic granitioids and volcanic rocks in South China: A response to tectonic evolution. *Episodes*, **29**: 26-33.

Zhou, Z., Xie, C., Xu, Q., and Gao, D., 2011. Geological and geochemical characteristics ofmiddle Triassic syenite-granite suite in Hainan Island and its geotectonic implications. *Geological Review*, **57** (4): 515-531 (in Chinese with English abstract).

(Edited by Chen Wenwen)